crystals

MDPI

Article

Effect of Process Conditions on Particle Size and Shape in Continuous Antisolvent Crystallisation of Lovastatin

John McGinty [1,2], Magdalene W. S. Chong [1,3], Andrew Manson [2], Cameron J. Brown [1], Alison Nordon [1,3], and Jan Sefcik [1,2,*]

[1] Future Manufacturing Research Hub in Continuous Manufacturing and Advanced Crystallisation, Technology and Innovation Centre, University of Strathclyde, 99 George Street, Glasgow G1 1RD, UK; john.mcginty@strath.ac.uk (J.M.); magdalene.chong@strath.ac.uk (M.W.S.C.); cameron.brown.100@strath.ac.uk (C.J.B.); alison.nordon@strath.ac.uk (A.N.)

[2] Department of Chemical and Process Engineering, University of Strathclyde, James Weir Building, 75 Montrose Street, Glasgow G1 1XJ, UK; andrew.manson@strath.ac.uk

[3] WestCHEM, Centre for Process Analytics and Control Technology (CPACT), Department of Pure and Applied Chemistry, University of Strathclyde, 295 Cathedral Street, Glasgow G1 1XL, UK

* Correspondence: jan.sefcik@strath.ac.uk

Received: 21 September 2020; Accepted: 9 October 2020; Published: date

1. Acquisition of Data for Calibration Model Building

To collect spectra for calibration model building, the UV-vis and IR probes were positioned into a 1 L jacketed STR. The temperature of the jacket was controlled by a Lauda Eco RE 420 water heater/chiller equipped with an external PT100 temperature probe that was inserted into the vessel. The mixing of acetone and water is exothermic, therefore temperature monitoring was used to confirm the calibration spectra are at 25 °C. A HEL Crystal Eyes DMS-2 Chemlog system equipped with a PT100 temperature probe and a turbidity probe were used to log the temperature and confirm the presence of solutions.

Dilution experiments were used to obtain samples at different lovastatin concentration and acetone/water composition. An initial solution of lovastatin in the desired acetone/water composition was prepared. The solution was transferred into the STR, ensuring the probes were submerged. The mass of material transferred into the STR was determined by the mass difference of the flask and contents before and after transfer into the STR. The contents were stirred at 200 rpm to prevent the formation of bubbles in the turbidity probe. The solvent composition (acetone mass fraction) and lovastatin concentration were determined by the composition of the material added to the STR. The first and subsequent two IR and UV-vis spectra upon reaching 25 °C were used to give triplicate spectra per sample for calibration model building.

For monitoring of the STR during the controlled antisolvent crystallisation experiments, the UV-vis spectra were acquired using an integration time of 62.8 ms and the IR spectra were acquired with a resolution of 2 cm^{-1} and at 60 s intervals. To apply the partial least squares (PLS) model to the IR spectra from the controlled antisolvent crystallisation experiments, the wavenumbers corresponding to the resolution of the spectra in the calibration model were selected.

The number of latent variables to use was determined by a venetian blinds cross validation procedure (3 splits). The minimal number of latent variables was selected that provided a suitable accuracy according to the root mean square error of cross validation (RMSECV).

2. UV Calibration Model Building

The calibration was built from 13 solution samples (triplicate spectra per sample). To focus on the process end region, the acetone/water composition covered is 0.40–0.76 acetone mass fraction and the range of the lovastatin concentration is 0.00–42.94 g/kg solvent (Figure S1). Four validation

samples (triplicate spectra per sample) were prepared, with a lovastatin concentration range of 1.71–28.65 g/kg solvent. All spectra were collected at 25 °C.

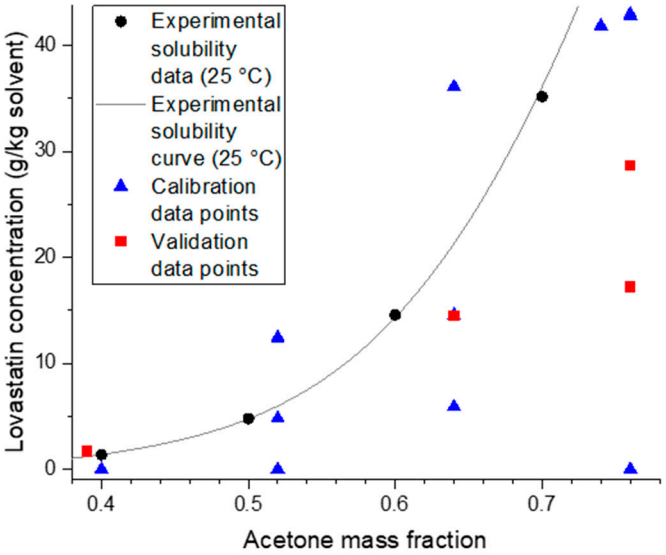

Figure S1. Experimentally determined solubility of lovastatin in acetone/water at 25 °C and the calibration and validation data points used for construction of a PLS model to predict the concentration of lovastatin by UV.

A PLS model with three latent variables (Table S1,Figure S2) was constructed using Savitzky-Golay derivatisation (1st derivative calculated using a 3-point filter width and a 2nd order polynomial) pre-processing with mean centring (Figure S3). The UV region 216-265 nm was selected for calibration building (Figure S2), which includes the lovastatin absorption bands (232, 239 and 247 nm in pure acetone) but excludes the remaining features from the broad acetone absorption. The features from the first derivative spectra dominate the loadings (Figure S4).

Table S1. Summary of model performance metrics – root mean square error (RMSE) and coefficient of determination (R^2).

	Calibration	Cross validation	Prediction
RMSE (g/kg solvent)	0.311	0.829	0.620
R^2	0.9997	0.9982	0.9986

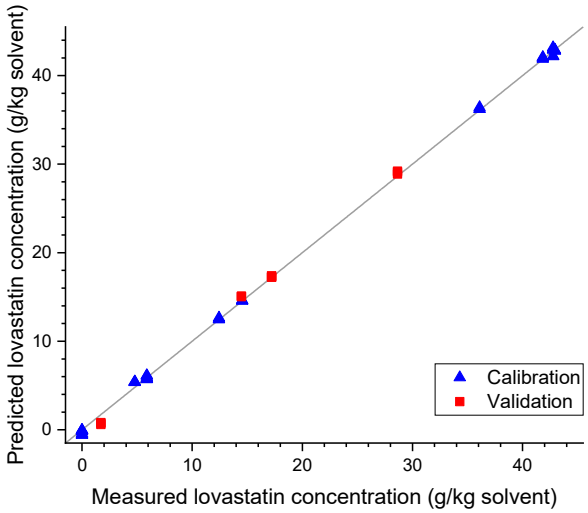

Figure S2. Actual *vs* predicted values of lovastatin concentration measured by UV.

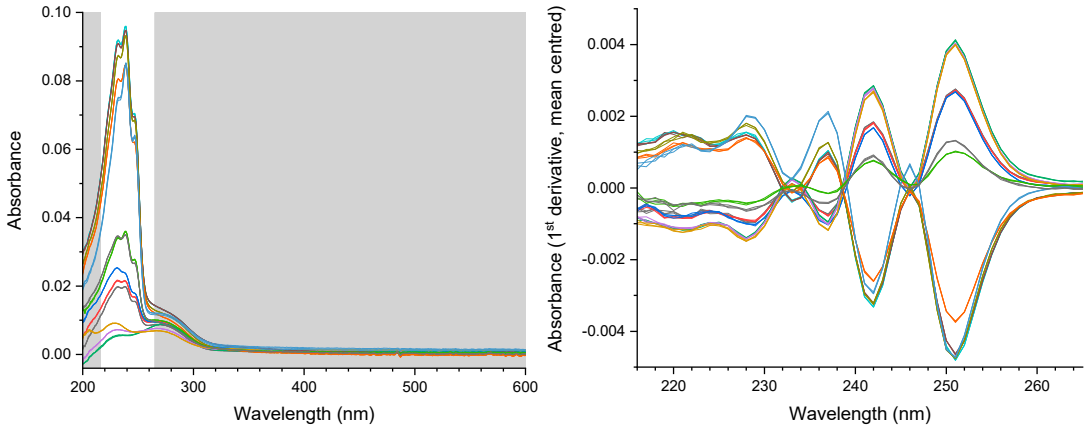

Figure S3. UV-vis calibration spectra with selected region for PLS model building selected in white (**left**) and after pre-processing (**right**).

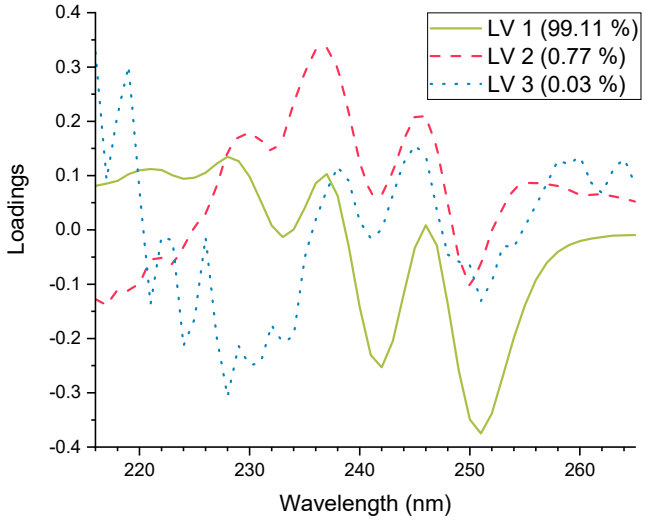

Figure S4. Loadings for each latent variable used in the PLS model to predict lovastatin concentration by UV.

3. IR Calibration Model Building

The calibration was built from 20 samples (triplicate spectra per sample) covering a range of 0.00–1.00 acetone mass fraction (Figure S5). For validation, 18 samples (triplicate spectra per sample) were prepared across the range 0.04–1.00 acetone mass fraction. The samples cover the full acetone mass fraction range that may be employed in the antisolvent crystallisation process.

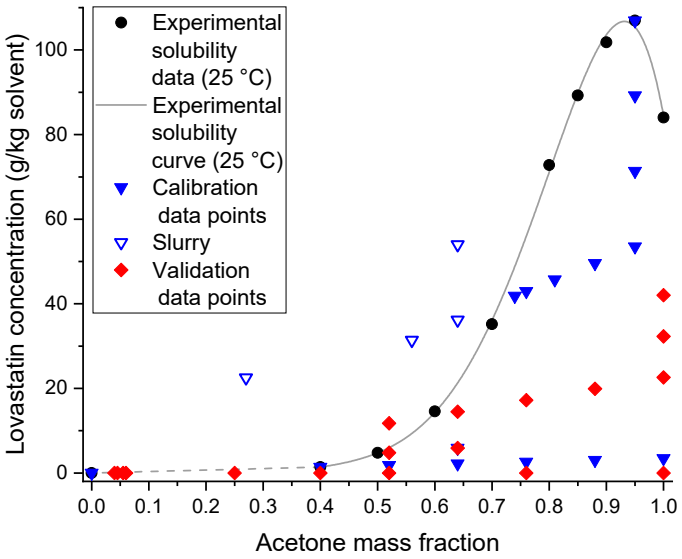

Figure S5. Experimentally determined solubility of lovastatin in acetone/water at 25 °C and the calibration and validation data points used for construction of a PLS model to predict the acetone mass fraction by IR. Where the calibration points are slurries the precise lovastatin concentration is unknown and the supersaturated concentration has been plotted.

A PLS model with three latent variables was constructed with mean centring of the spectra (Table S2, Figure S6). The region 1778.2–732.9 cm^{-1} was selected for calibration building. Within this region distinct acetone peaks are observed at 1711, 1437, 1421, 1358, 1219 and 1092 cm^{-1}. There are broad water peaks at 1647 cm^{-1} and below 891 cm^{-1} that are captured within the region (Figure S7). The acetone and water features contribute to the loadings for each latent variable (Figure S8).

Table S2. Summary of PLS model performance metrics for prediction of solvent composition by IR.

	Calibration	Cross validation	Prediction
RMSE (acetone mass fraction)	0.0036	0.0076	0.0052
R^2	0.9996	0.9982	0.9997

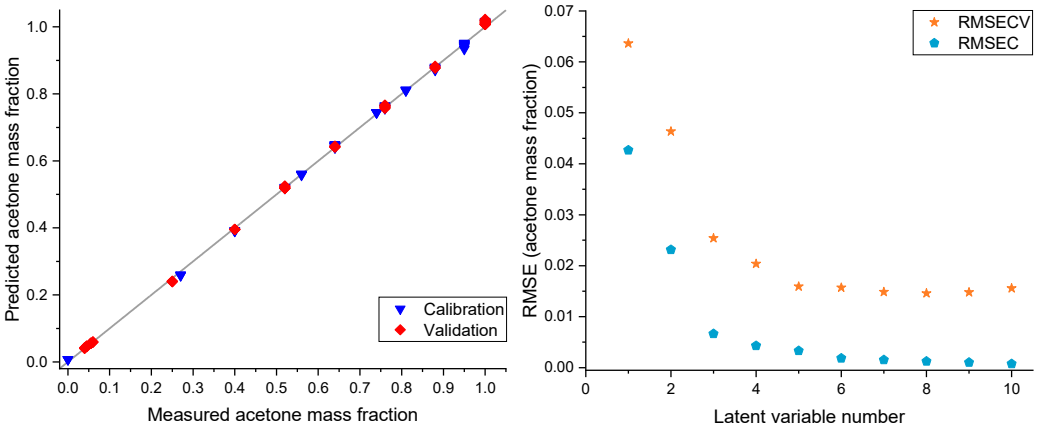

Figure S6. Actual *vs* predicted values of acetone mass fraction of acetone/water mixtures measured by IR (**left**). RMSE of calibration and cross validation against latent variable number (**right**).

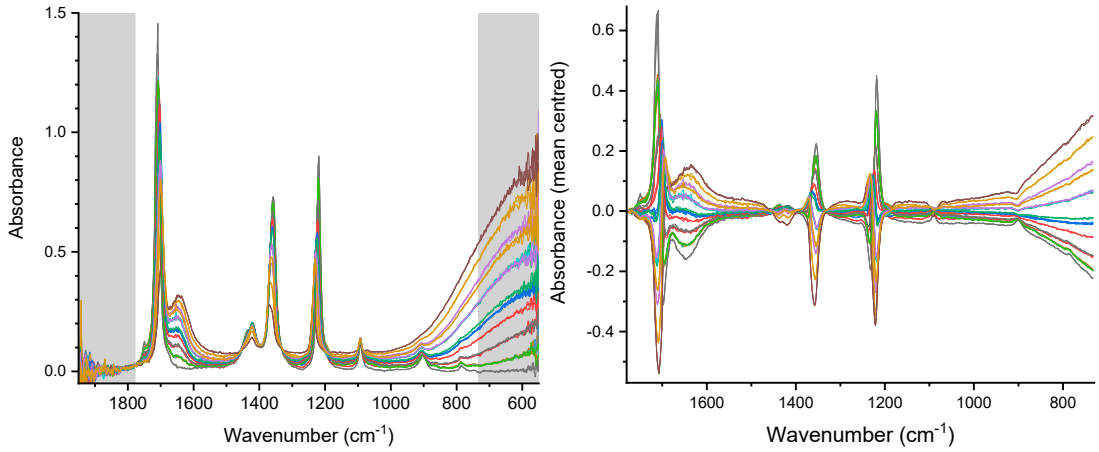

Figure S7. IR calibration spectra with selected region for PLS model building selected in white (**left**) and after pre-processing (**right**).

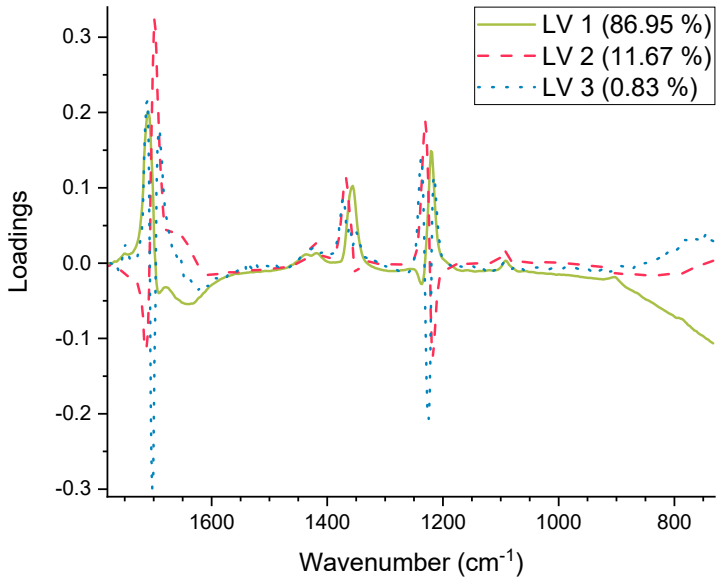

Figure S8. Loadings for each latent variable used in the PLS model to predict acetone mass fraction by IR.

4. Full UV and IR Online Monitoring Results

During the antisolvent crystallisation experiments, in situ monitoring of the 1L STR was carried out using FBRM, UV-vis and IR. Predicted values for the concentration of lovastatin and acetone mass fraction were obtained from the UV and IR PLS models respectively (Table S3). For the offline sample, the lovastatin concentration was calculated from the slurry mass and dry crystals mass, with the assumption the offline sample taken is representative of the bulk material in the 1 L STR. The expected acetone mass fraction is determined from the ratio of the solution and antisolvent feeds.

Table S3. Experimental lovastatin concentration and acetone mass fraction predicted by UV and IR respectively. A lovastatin concentration was calculated for the offline sample and the acetone mass fraction calculated from the ratio of the solution and antisolvent feeds.

[LOV] predicted by UV (g/kg solvent)	[LOV] calculated for offline sample (g/kg solvent)	Acetone mass fraction predicted by IR	Expected acetone mass fraction for solution:antisolvent ratio

Exp 1	0.17	11.27	0.42	0.43
Exp 2	−6.72	7.26	0.43	0.43
Exp 3	-	21.37	-	0.58
Exp 4	23.99	27.97	0.65	0.66
Exp 5	-	20.33	-	0.43
Exp 6	−1.74	13.70	0.45	0.43
Exp 7	-	21.80	-	0.58
Exp 8	-	31.63	-	0.66

There is good agreement of the acetone mass fractions predicted by IR with the expected experimental acetone mass fraction. There are larger discrepancies in the lovastatin concentration predicted by UV and that calculated for the offline sample. There appears to be three outcomes from the concentration measurements: (1) quantitative predictions with no obvious fouling, (2) qualitative predictions where general trends correlate well with other experimental observations, and (3) inaccurate predictions where there has likely been significant probe fouling. The propensity for fouling results from the combination of factors selected for control of lovastatin particle size and shape.

Experiment 1 uses a high pre-nucleation supersaturation, the short induction time results in nucleation occurring before filling of the STR. Thus, the filling of the STR with heterogeneous material leads to a higher likelihood of fouling compared to Experiment 4. Fouling is observed in the initial IR spectra for this experiment, which may contribute to the higher acetone mass fraction predicted initially (Figure S9). Consistent acetone mass fractions of 0.42 (7 minutes onwards) are predicted by IR for this experiment. The initial concentration prediction from UV is high (38.94 g/kg solvent, Figure S9), with the expected pre-nucleation concentration being 43.79 g/kg solvent. This value appears reasonable; however, fouling would result from either filling of the STR with heterogeneous material or deposition of crystallised material onto surfaces from the short induction time at this supersaturation. Despite the observed fouling, the concentration trends predicted by UV are reasonable with respect to the trends observed by FBRM. Therefore, despite the deficiencies in quantitative data, qualitative trending of the solute concentration is achieved.

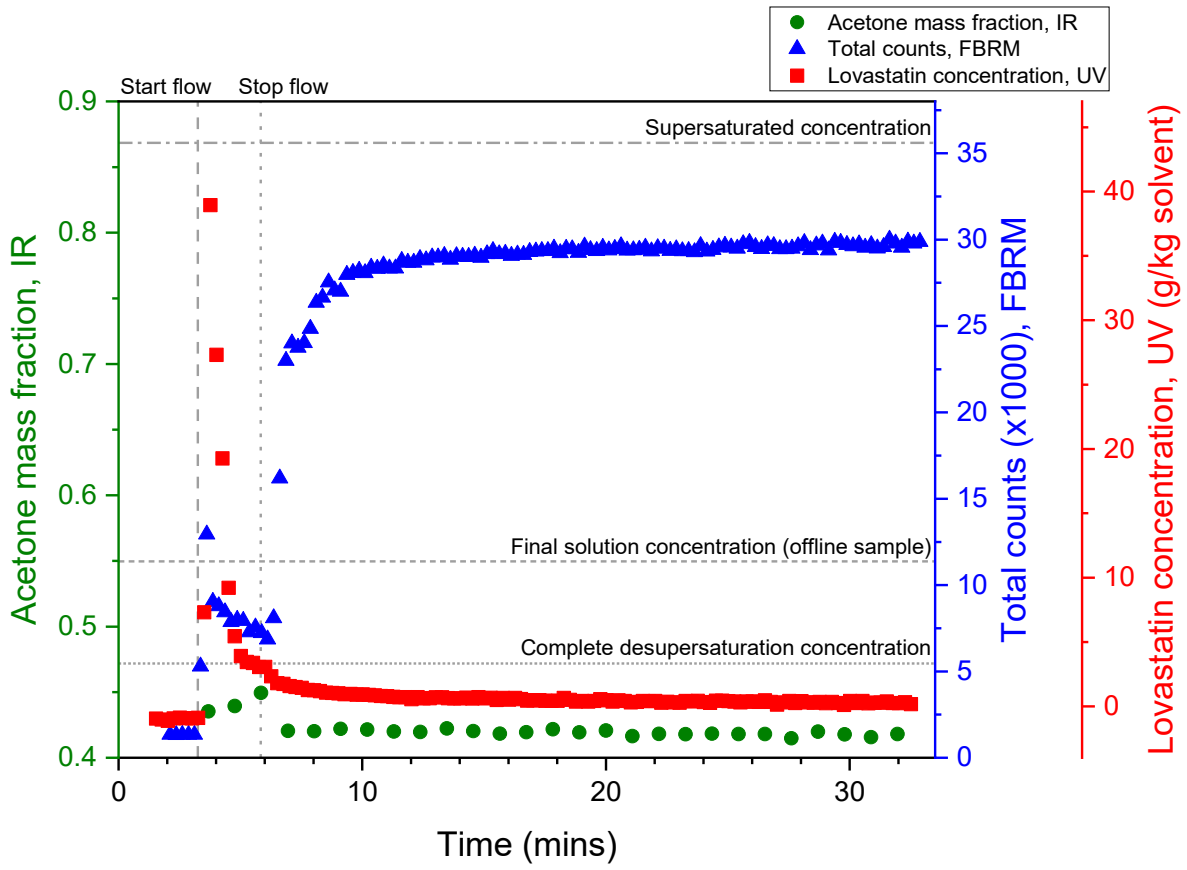

Figure S9. Predicted acetone mass fraction by IR, predicted lovastatin concentration by UV and total counts from FBRM from monitoring of the STR during Experiment 1. Experimental events and expected concentrations have been outlined.

Experiments 2 and 6 feature a combination of high pre-nucleation supersaturation and high flow rate. The highest likelihood for fouling during filling of the STR is expected, with the use of sonication in Experiment 6 increasing this further. There is evidence of fouling in the initial IR spectra for both experiments and the UV spectra look unusual and do not resemble the calibration spectra. Two filling events were used for Experiment 6, which is reflected in all of the measurement trends (Figure S10). The second filling event was thought to be required during the experimental run to ensure that all of the probes were sufficiently submerged in the solution (this requirement was thought to outweigh the risk of disturbing the crystallisation environment). Whilst the general trends for the predicted solute concentration by UV in both experiments appear to correspond to experimental events, the negative predictions strongly suggest that both Experiments 2 and 6 are examples of scenarios where the extent of probe fouling has significantly affected the quality of the spectra collected. Quantitatively, the predictions are below the complete desupersaturation concentration, which has been taken as the experimental solubility.

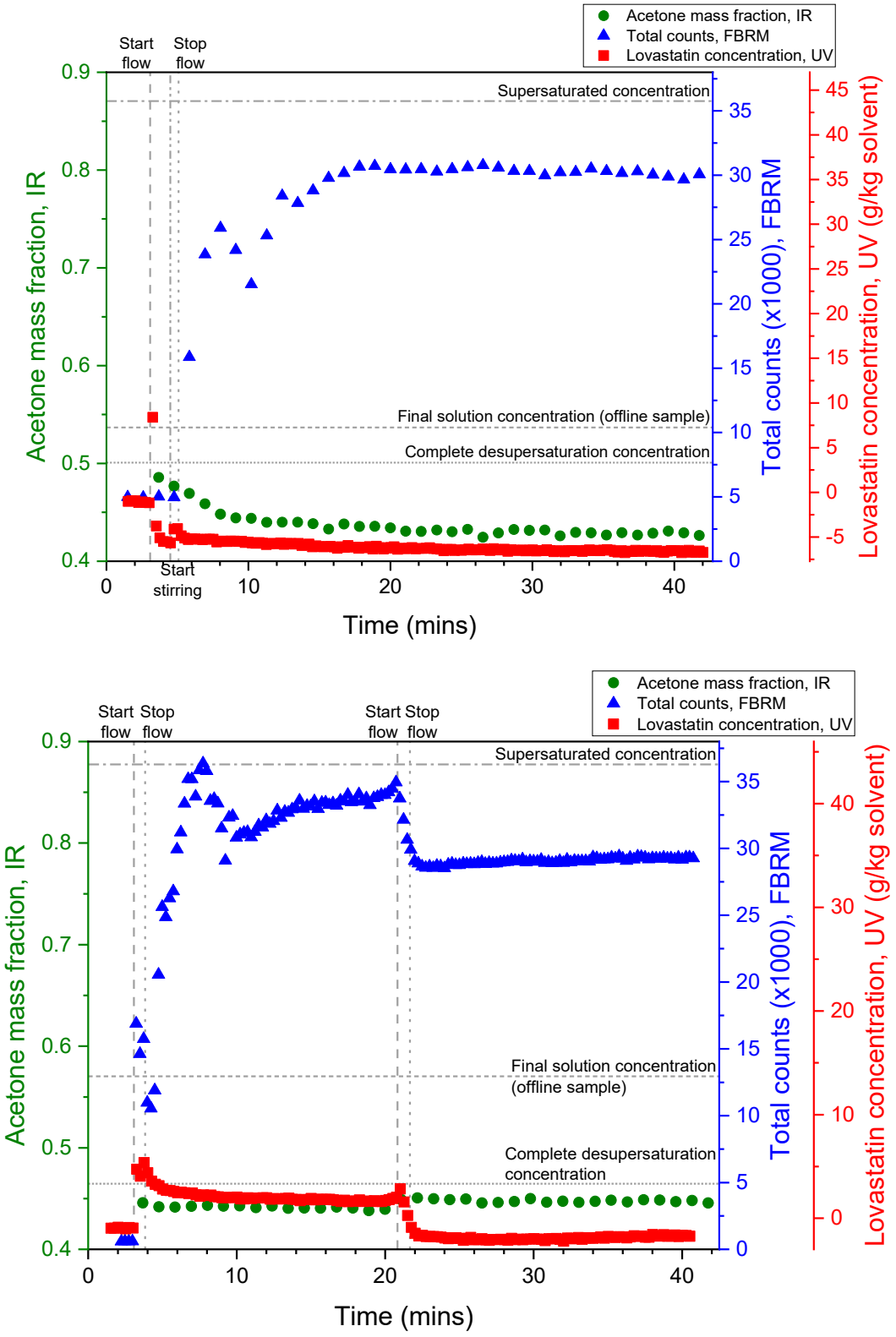

Figure S10. Predicted acetone mass fraction by IR, predicted lovastatin concentration by UV and total counts from FBRM from monitoring of the STR during Experiments 2 (**top**) and 6 (**bottom**). Experimental events and expected concentrations have been outlined.

Whilst fouling was evident (visually) in some of the IR spectra, it does not appear to have significant impact on the final predictions. This is likely because the intensity of the lovastatin features resulting from fouling are much lower than those from the solvent. Additionally, the loadings for each latent variable in the PLS model are dominated by solvent features (Figure S8), which the

lovastatin features do not contribute towards. Despite the evident fouling observed in the IR, the main solvent features are still detected. Fluctuations in the absorbance of the lowest intensity acetone vibrational band at 1092 cm^{-1} are smaller in comparison to the changes in observed in absorbance that are attributable to lovastatin. It would be reasonable to suggest that the nature of the fouling on the ATR probes is a thin layer that does not fully obscure the penetration of the evanescent wave.

In the case of the UV-vis measurements, the extent of fouling on the ATR probe significantly impacts the quality of the measured spectra. The calibration was constructed using solutions, with the reasonable assumption that the ATR probe will only sample the liquid phase in a slurry. It appears the fouling issues are inherent to the experimental procedure, resulting in ATR measurements that are not representative of the liquid phase. For all of these experiments, where UV-vis, IR and FBRM monitoring were present, the fouling indices of the FBRM measurements are initially very high (exceeding 10%). These remain high for some time after flow has been stopped. Alternatively, non-invasive methods would similarly be limited as similar obscuration issues would arise if fouling occurs on the surfaces of the 1L STR.

5. FBRM Online Monitoring Results

In addition to spectroscopic tools, an FBRM probe was used to monitor the particle size during the crystallisation process. A comparison of the chord length distributions (CLDs) at the end of the crystallisation processes are shown in Figure S11. The comparison shows very little difference between the experiments.

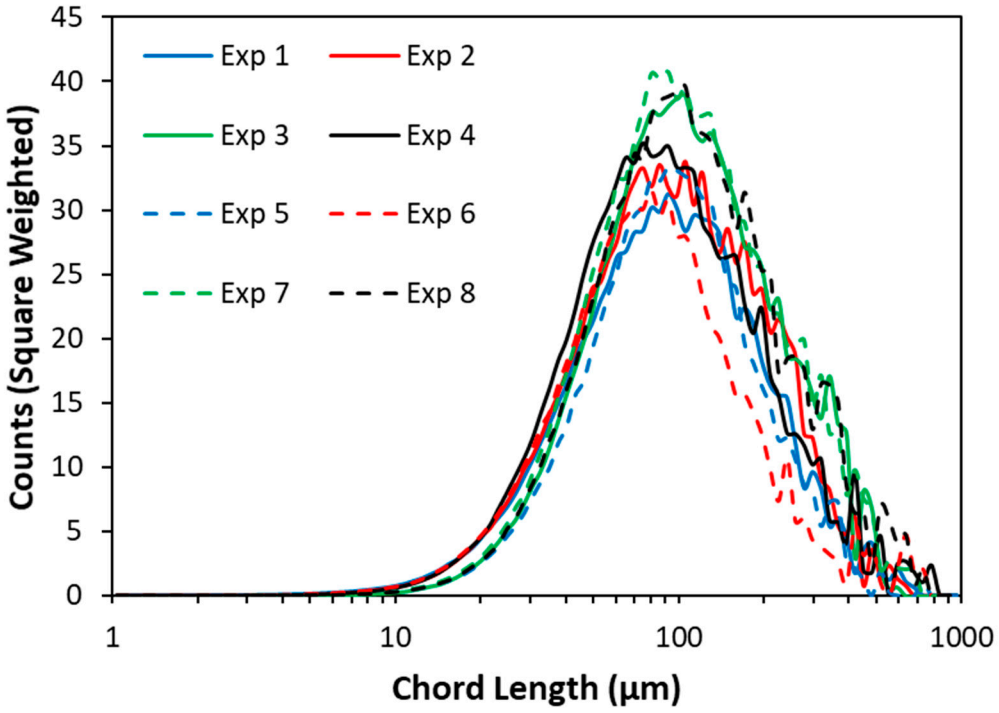

Figure S11. Comparison of chord length distributions at the end of each experiment. The FBRM data is from the macro mode and the distributions are square weighted.

In order to assess if the FBRM probe had significantly fouled in any of the experiments the fouling index values were plotted and compared in Figure S12. It can be seen from this comparison that for each experiment the fouling index is at its highest at the beginning and decreases over time which is most likely because the agitation in the vessel gradually washes away deposited material over time. It can also be seen from this comparison that in all the experiments the FBRM probe is at least partially fouled by the end with the fouling index ranging from 7.5 to 20%. When comparing the fouling indices at the end of each experiment, experiment 4 exhibits the joint lowest value which

is expected as this experiment has the least intense nucleation environment (lowest supersaturation and no ultrasound applied) whereas experiment 6 has among the greatest values which is also expected as this experiment has the most intense nucleation environment (highest supersaturation and ultrasound applied). Typically, the value of fouling index which corresponds to significant fouling is thought to be 10% which would mean that the vast majority of the experiments do indeed exhibit significant fouling.

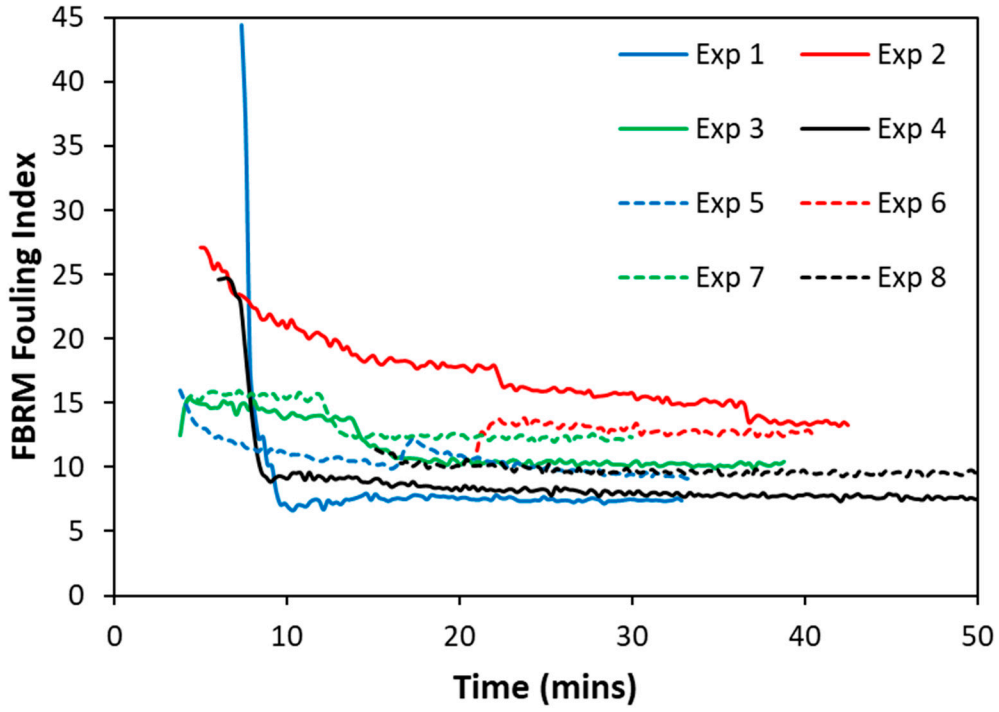

Figure S12. Comparison of fouling index values from FBRM over the course of each experiment. The data displayed begins from the point at which the FBRM probe was thought to be submerged in the solution.

6. Photographs of the Antisolvent Crystallisation Experimental Setup

A photograph of the full antisolvent crystallisation experimental setup (not running) is shown in Figure S13a. In this photograph, the material flows from right to left when in operation. Figure S13b shows the X-mixer connected to the tubing in the ultrasonic bath. Figure S13c shows the orientation of the PAT probes inside the 1 L jacketed STR. Figure S13d shows a close-up view of the X-mixer and Figure S13e shows a close-up view of the Y-splitter. The X-mixer and the Y-splitter are simple tube connectors with smooth bores and 1/8th in. internal diameter.

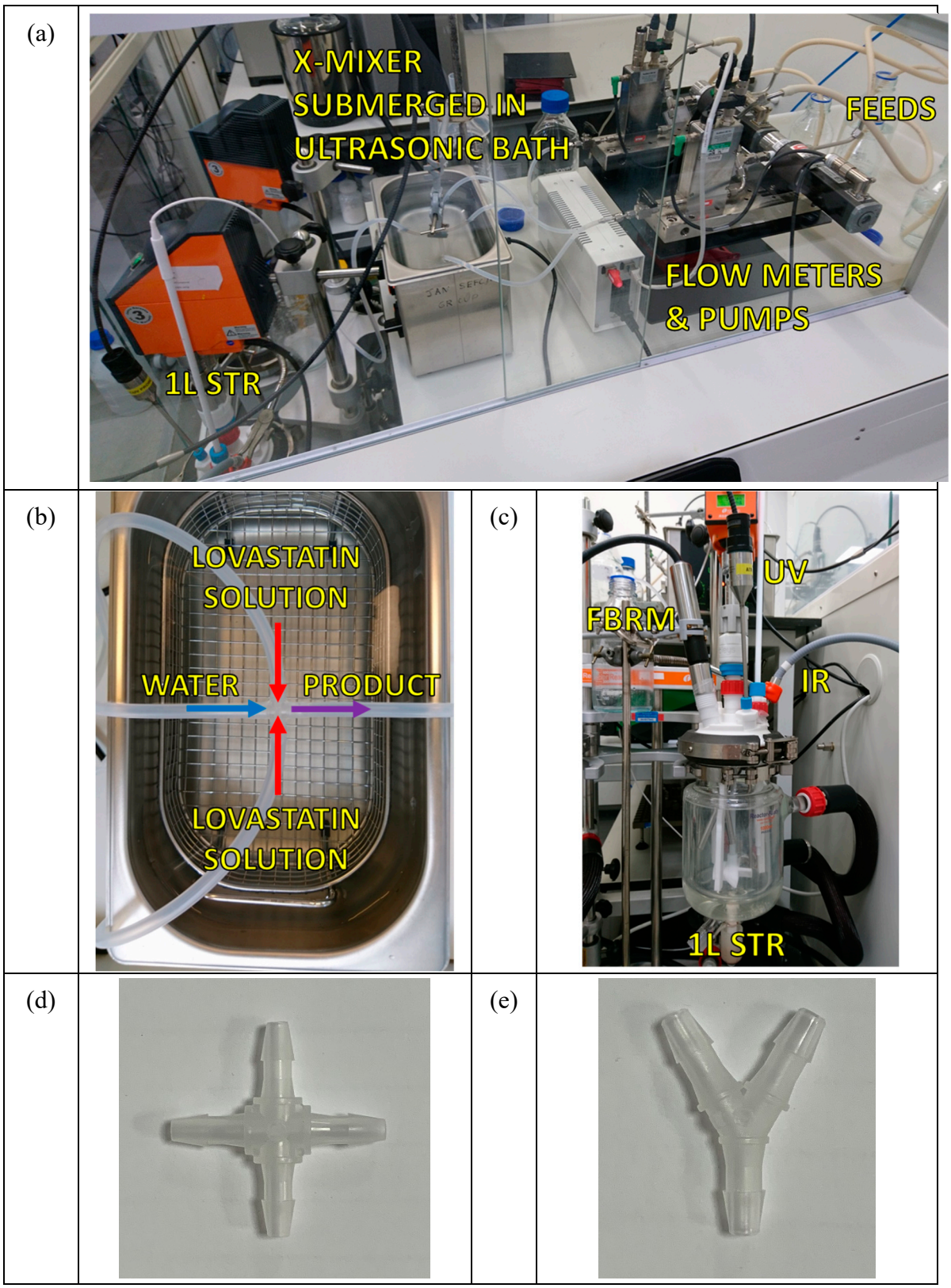

Figure S13. Photographs of (**a**) the full antisolvent crystallisation experimental setup (not running), (**b**) the X-mixer connected to the tubing in the ultrasonic bath, (**c**) a close-up view of the 1 L jacketed STR with the PAT probes inserted, (**d**) a close-up, top-down view of only the X-mixer, and (**e**) a close-up, top-down view of only the Y-splitter.